Analytical and Numerical Methods in Mechanical Design
Vol.1, Issue 1, Winter & Spring 2022, 71-87

Investigation of The Mechanism of Change of Concrete Modulus Matrix in Monotonic Loading and its Numerical Analysis

Farzad Peyman[1,*]

[1] *Department of Civil Engineering, QazvinBranch,Islamic Azad University Qazvin, Iran*

Received: 08 February 2022- Accepted: 12 April 2022

*Corresponding author : *f.peyman@srbiau.ac.ir*

Abstract

The primary purpose of studying the behavior of concrete is to calculate its strength and deformation under environmental conditions and loading. In this regard, due to the structure and nature of concrete, non-isotropic in its experimental behavior at different loads is observed, considered in this research. Accordingly, by assuming a different linear elastic behavior in each loading increment and the experimental results, an attempt has been made to define a numerical linear-nonlinear behavior for concrete. Therefore, proportional numerical functions are defined based on the damage in the modulus of elasticity and the changes in the Poisson ratio of the concrete tested in monotonic loading types, the coefficients obtained from the related experimental results. The computational effects of these functions during the analytical method of the research cause the experimental behavior of concrete to be converted to numerical behavior. The validity of this numerical method is based on calibration and comparison with experimental results. In addition to hardening behavior, this numerical analysis can define softening behavior.

***Keywords*:** Concrete, Non-isotropic, Damage, Monotonic Loading, Hardening, Softening

1. Introduction

Concrete is one of the most important materials used in construction. This material, which consists of aggregates, cement, water, and other additives, has established its position as a building material over time. Today, few buildings can be found that have not used concrete in the body. On the other hand, the design and implementation of concrete structures require proper analysis against the loads, and its accuracy depends on the type and importance of the structures. For example, the analysis of a multi-story concrete building is different in every way from the analysis of a concrete dam or concrete cooling tower. In line with this analysis, the behavior of concrete should be carefully studied. Moreover, behavioral models closer to reality should be researched and defined. Using these models to analyze concrete structures while making the design more economical can provide more security for humans and the surrounding areas.

Concrete can exhibit complex behavior under load. The main reason is nonlinear behavior due to the onset, growth, and spread of cracks. Other cases such as; Water to cement ratio, material, shape and grain size of stone materials, void ratio, concrete age, non-homogeneous and non-isotropic, type and speed of loading, and stress path are essential factors in this field. For these reasons, it becomes difficult to predict the behavior and determine the deformation of concrete at different loads [1-3].

Many analytical models have been proposed to define and predict the behavior of concrete. However, some of them cannot express all the properties and characteristics of behavior, and others are so difficult that their use in practical cases is costly and eliminated. Studies show that recent models can be divided into continuous and discontinuous groups. In continuous models, it is assumed that the material operates seamlessly and there is no discontinuity, including cracking, slipping, separation or failure. In discontinuous models, the material is thought of as a set of particles that can affect each other's motion.

Continuous models into two subgroups; macro, based on theories of paste or damage or a combination of both [4-10], and are divided into mesoscopic such as micro-plane or multi-laminate models [11-22]. Discontinuous models also lead to a subset called micro models, such as discrete particle models [23-25].

In macro models, material behavior is defined based on the direct relationship between stress and strain tensors [26-34]. However, in mesoscopic models, the material's behavior is clearly defined by the relationship between stress and strain vectors on planes, known as micro-plane or multi-laminate planes [35-42]. In discontinuous models, the material's behavior is simulated based on the definition of inter particle forces due to their motion on each other and their use in

the equation of motion and numerical solution. In discontinuous models, the material's behavior is simulated by numerical solution based on the definition of inter particle forces due to their motion relative to each other and the use of motion equation [43-49].
In this comparison, discontinuous models define the behavior of materials better than other models due to the precise and close to reality type of payment. However, using them can be difficult, complicated, and costly for engineering purposes. On the other hand, macro models based on stress or strain invariants cannot simulate the behavioral properties of direction-dependent materials. It is impossible to store information dependent on different directions by these models. Therefore, it seems that microscopic models are a logical and intermediate solution between the two groups. For these reasons, in the present research, a method based on damage theory has been developed that can be used in multi-laminate models for numerical analysis of concrete behavior at monotonic loading [39].

2. Numerical analysis of concrete behavior

The main purpose of studying the behavior of different types of concrete in different environmental conditions and loads is to calculate their strength and deformation. In this regard, and based on the experimental results, a kind of non-isotropic behavior of concrete is observed, which is examined numerically in this research. Based on the theory of damage and change, the proposed numerical method is defined to predict the behavior of different categories of concrete in monotonic loading types. Its calibration is also based on valid experimental results such as; tri-axial compression, uni-axial compression, and tensile axial are obtained.

2.1. Hypotheses and parameters used in numerical analysis

In this method, based on the principal stress space in monotonic loading tests, in each load increase increment, the behavior of concrete can be considered homogeneous, isotropic, linear elasticity, and, of course, different from the previous and next load increment. In other words, the perspective of hypo-elastic behavior was considered a criterion and, depending on the type of experiment, the general form of damage and change functions in numerical analysis was proposed. In this way, the non-isotropic behavior of concrete in pressure, tension, and shear can be defined.
To begin with, in each loading increment *i*, the relationship between the stress and strain vectors in the principal stress space can be represented as Equation (1).

$$\begin{Bmatrix}\sigma_{1i}\\ \sigma_{2i}\\ \sigma_{3i}\end{Bmatrix}=\frac{E_i}{(1+\nu_i)(1-2\nu_i)}\begin{bmatrix}1-\nu_i & \nu_i & \nu_i\\ \nu_i & 1-\nu_i & \nu_i\\ \nu_i & \nu_i & 1-\nu_i\end{bmatrix}\begin{Bmatrix}\varepsilon_{1i}\\ \varepsilon_{2i}\\ \varepsilon_{3i}\end{Bmatrix} \quad (1)$$

For a cylindrical sample in a triaxial compression test, at the deviator stress increment stage, Equation (1) is rewritten as (2).

$$\begin{Bmatrix}\sigma_{1i}\\ \sigma_{3i}\\ \sigma_{3i}\end{Bmatrix}=\begin{Bmatrix}\sigma_3\\ \sigma_3\\ \sigma_3\end{Bmatrix}+\begin{Bmatrix}\Delta\sigma_i\\ 0\\ 0\end{Bmatrix}=\begin{Bmatrix}\sigma_3\\ \sigma_3\\ \sigma_3\end{Bmatrix}+\frac{E_i}{(1+\nu_i)(1-2\nu_i)}\begin{bmatrix}1-\nu_i & \nu_i & \nu_i\\ \nu_i & 1-\nu_i & \nu_i\\ \nu_i & \nu_i & 1-\nu_i\end{bmatrix}\begin{Bmatrix}\varepsilon_{1i}\\ \varepsilon_{3i}\\ \varepsilon_{3i}\end{Bmatrix} \quad (2)$$

From the expansion of Equation (2), Equations (3) and (4) are obtained.

$$\sigma_{1i}=\sigma_3+\frac{E_i}{(1+\nu_i)(1-2\nu_i)}\cdot[(1-\nu_i)\varepsilon_{1i}+2\nu_i\varepsilon_{3i}] \quad (3)$$

$$\sigma_{3i}=\sigma_3+\frac{E_i}{(1+\nu_i)(1-2\nu_i)}\cdot(\nu_i\varepsilon_{1i}+\varepsilon_{3i}) \quad (4)$$

In which:

$$\nu_i=-\frac{\varepsilon_{3i}}{\varepsilon_{1i}} \quad (5)$$

In these equations and each loading increment *i*:

σ_{3i}=Minor principal stress in every increment
σ_{2i}= Middle principal stress in every increment
σ_{1i}=Major principal stress in every increment
ε_{3i}=Minor principal strain in every increment
ε_{2i}=Middle principal strain in every increment
ε_{1i}=Major principal strain in every increment
σ_3=Minor principal stress
E_i=Modulus of elasticity in every increment
ν_i=Poisson ratio in every increment

Equation (5) in Equation (4) will lead to the reality of Equation (6).

$$\sigma_{3i} = \sigma_3 + \frac{E_i}{(1+\nu_i)(1-2\nu_i)} \cdot (-\varepsilon_{3i} + \varepsilon_{3i}) = \sigma_3 + 0 = \sigma_3 \tag{6}$$

In the following, parameters such as mean and shear stresses and volumetric strain in each loading increment are defined as Equations (7) to (9).

$$p_i = \frac{\sigma_{1i} + 2\sigma_{3i}}{3} = \frac{\sigma_{1i} + 2\sigma_3}{3} \tag{7}$$

$$q_i = \sigma_{1i} - \sigma_{3i} = \sigma_{1i} - \sigma_3 = \Delta\sigma_i \tag{8}$$

$$\varepsilon_{vi} = \varepsilon_{1i} + 2\varepsilon_{3i} = (1-2\nu_i) \cdot \varepsilon_{1i} \tag{9}$$

In which:

q_i=Deviatoric stress in every increment
p_i=Mean stress in every increment
ε_{vi}=Volumetric strain in every increment

From the placement of Equation (3) in Equations (7) and (8) and the use of Equations (9) and (5) in them, we can conclude Equations (10) and (11).

$$p_i = \frac{q_i}{3} + \sigma_3 \tag{10}$$

$$q_i = \frac{E_i}{1+\nu_i} \cdot (\varepsilon_{1i} - \varepsilon_{3i}) = E_i \cdot \varepsilon_{1i} \tag{11}$$

Thus, the changes in the modulus of elasticity and the Poisson's ratio of concrete during the static triaxial compression test are determined from Equations (12) and (5).

$$E_i = \frac{\sigma_{1i} - \sigma_3}{\varepsilon_{1i}} = \frac{q_i}{\varepsilon_{1i}} \tag{12}$$

To observe the damage in the modulus of elasticity and the change in the Poisson ratio during the behavior of concrete at monotonic loading, we can initially use the experimental results of different samples of C28.6 class concrete at confining pressures different from the characteristics of Figure 1 [50]. The experimental results of Figure 1 show that the strength of concrete increases with increasing confining pressure.

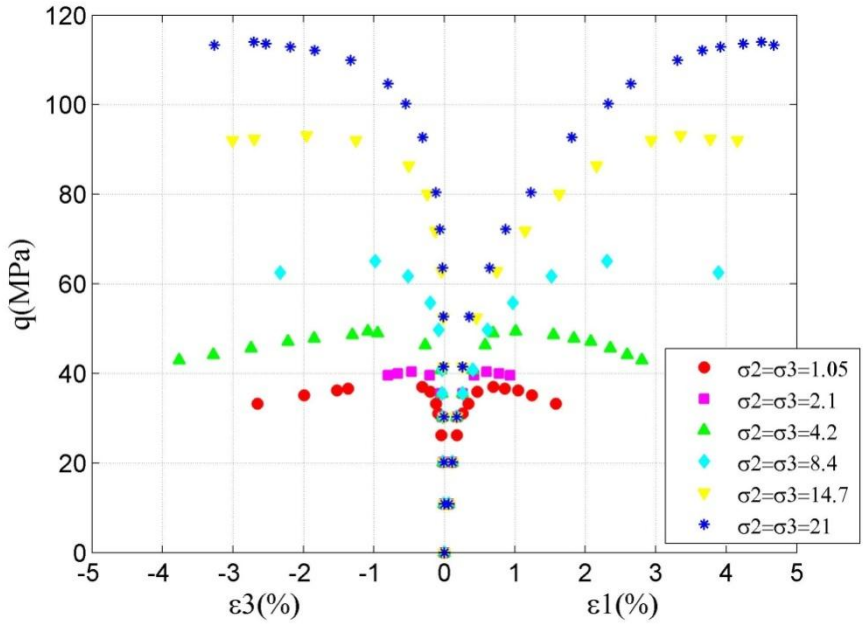

Fig. 1.Behavioral curves in monotonic tri-axial compression tests on C28.6 class concrete samples at different Confining pressures [50]

For concrete samples of class C28.6, changes in the modulus of elasticity can be calculated using Equation (12) and plotted against axial strain, as shown in Figure 2.

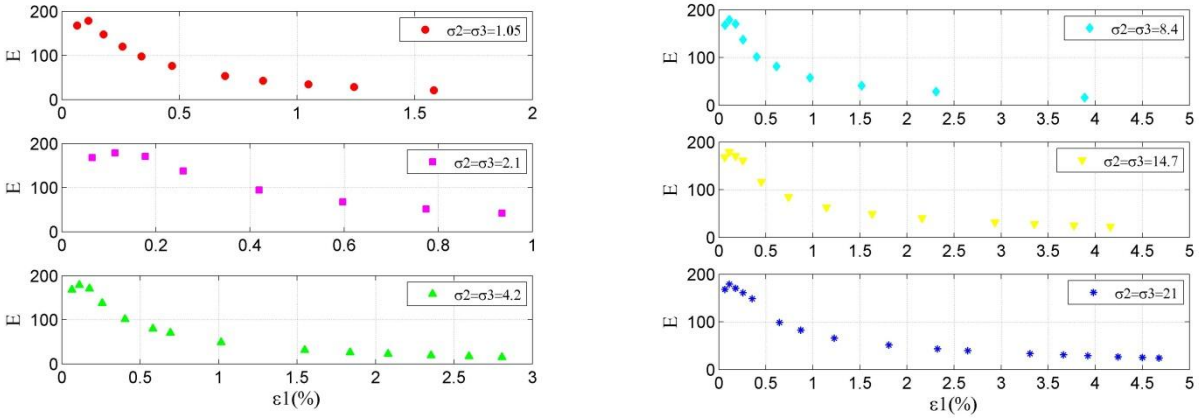

Fig. 2.Modulus of elasticity changes with increasing axial strain in monotonic tri-axial compression tests on C28.6 class concrete samples at different confining pressures

The graphical results of Figure 2 for the samples of this concrete class show that the modulus of elasticity, after a slight initial increase, continues to be damaged and decreases with increasing axial strain. This is the onset of nonlinear behavior, cracking, growth, and propagation of cracks.

For concrete samples of class C28.6, changes in the Poisson's ratio can be calculated using Equation (5) and plotted against axial strain, as shown in Figure 3.

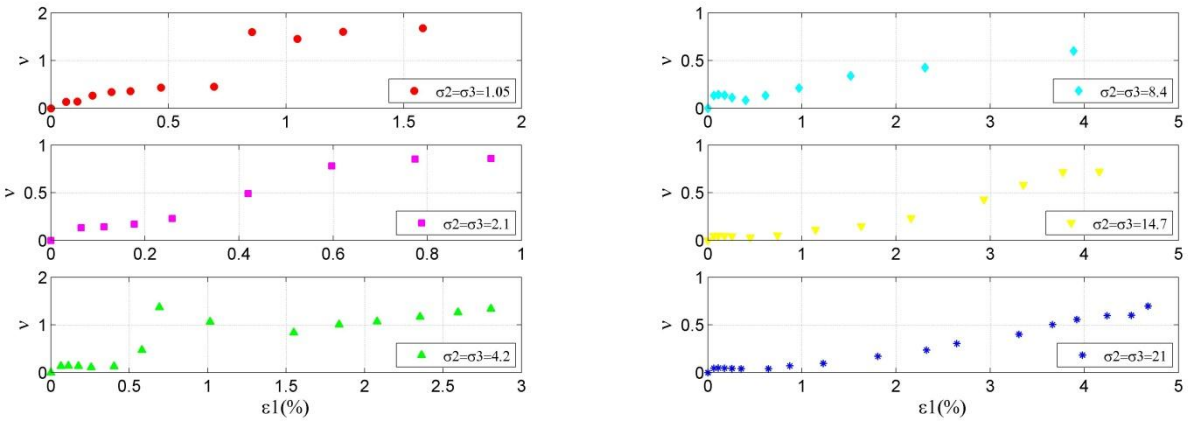

Fig. 3. Changes in the Poisson ratio with increasing axial strain in monotonic triaxial compression tests on C28.6 class concrete samples at different confining pressures

The graphical results of Figure 3 show that the Poisson ratio increases uniformly during the first three samples at a higher rate and amplitude than the second three samples during monotonic loading and with increasing axial strain. This is due to the confining pressure increase on the one hand and the onset of cracking, growth, and expansion of the cracks on the other hand.
Thus, the definition of relationships for damage to the modulus of elasticity and changes in the Poisson ratio is the criterion for numerical analysis in this research, which is presented below.

2.2. Defining numerical relationships of damage and changes

Based on the study conducted in this research, defining the N parameter according to Equation (13) can be used.

$$N = log[\frac{p}{\varepsilon_1 \cdot (1+\sigma_3)}] \quad for \quad (\varepsilon_1 > 0) \tag{13}$$

This initiative makes it possible to define the resulting experimental curve with a three-coefficient mathematical function according to Equation (14) by calculating and plotting the N versus ε_1 variations for the experimental samples.

$$f(\varepsilon_1) = A \cdot (\varepsilon_1)^B + C \tag{14}$$

In this regard, f is a function that can express the effect of axial strain on damage in the modulus of elasticity. Numerical coefficients A, B, and C are also obtained based on the numerical function f on the experimental variations N.
Equation (10) in Equation (13) and applying Equation (14), Equation (15) can be concluded.

$$N = log[\frac{\frac{q}{3}+\sigma_3}{\varepsilon_1 \cdot (1+\sigma_3)}] = f(\varepsilon_1) \quad \Rightarrow$$
$$q = 3[\varepsilon_1 \cdot (1+\sigma_3) \cdot 10^f - \sigma_3] \tag{15}$$

And by placing Equation (15) in Equation (12), Equation (16) is obtained.

$$E = 3[(1+\sigma_3) \cdot 10^f - \frac{\sigma_3}{\varepsilon_1}] \tag{16}$$

Numerical Equation (16) defines the trend of changes in the modulus of elasticity E in each loading increment i in terms of the principal strain ε_1.
Following the studies conducted in this research, it is better to start the Poisson's ratio changes during the experiment by defining the M parameter according to Equation (17).

$$M = log(-\frac{\varepsilon_3}{1+\varepsilon_1}) \quad for \quad (\varepsilon_3 < 0) \tag{17}$$

By calculating and plotting the changes of M versus ε_1 for the experimental samples, the resulting experimental curve can be defined by a four-coefficient mathematical function according to Equation (18).

$$g(\varepsilon_1) = a \cdot (\varepsilon_1)^b + c \cdot tanh(d \cdot \varepsilon_1) \tag{18}$$

In this regard, g is a function that can represent the effect of axial strain on the Poisson ratio. Numerical coefficients a, b, c, and d are also obtained based on the mathematical function g on the experimental variations M.
Thus, using Equation (5) in Equation (17) and applying Equation (18), we can conclude Equation (19).

$$\begin{aligned} &M = log(\frac{\nu \cdot \varepsilon_1}{1+\varepsilon_1}) = g(\varepsilon_1) \quad \Rightarrow \\ &\nu = 10^g \cdot (1+\frac{1}{\varepsilon_1}) \end{aligned} \tag{19}$$

Numerical Equation (19) defines the rate of change of the Poisson ratio in each loading increment i in terms of principal strain.

2.3. Numerical analysis process

In summary, the numerical analysis process considered in this research can be expressed as follows:

- Based on the experimental results of monotonic loading on the concrete sample, N and M parameters are calculated according to Equations (13) and (17). Their variations against axial strain ε_1 are plotted.
- From Equation (14) on the plotting curve obtained from Equation (13), the numerical coefficients A, B, and C are calculated, and the function f is defined.
- From Equation (18) on the plotting curve obtained from Equation (17), the numerical coefficients a, b, c, and d are calculated, and the function g is defined.
- By defining the numerical functions f and g, the modulus of elasticity E and the Poisson's ratio ν in each loading increment i are determined from Equations (16) and (19).
- Lateral strain ε_3 and volumetric strain ε_v in loading increment i are calculated from equations (5) and (9).
- The mean and shear stress p and q are determined from equations (10) and (11).

The recent analytical process algorithm is shown in the flowchart of Figure 4.

3. Examining the results of numerical analysis

In this section, the validity of the proposed numerical analysis is examined. For this purpose, calibration and comparison with related experimental results are used.

3.1. Calibration and comparison of numerical analysis results with the tri-axial compression test

For starters, the results of the tri-axial compression test of C28.6 class concrete samples at different confining pressures can be used [50]. The experimental behavior of recent concrete samples is converted to numerical behavior and compared with each other, based on the proposed algorithm of Figure 4 as follows.

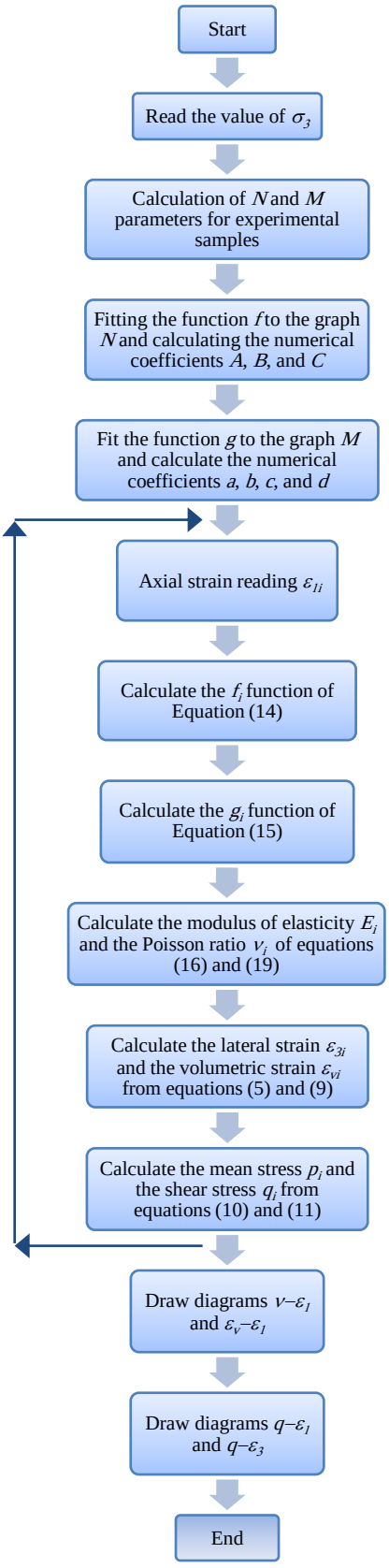

Fig. 4. Flowchart of numerical analysis

Parameter N is calculated from experimental results, and according to Equation (13), its changes against the axial strain ε_1 are plotted. Then, according to Figure 5, from the fit of the numerical relation 14 on the resulting curves, the numerical coefficients A, B and C are determined and are inserted in Table 1 to define the numerical function f.

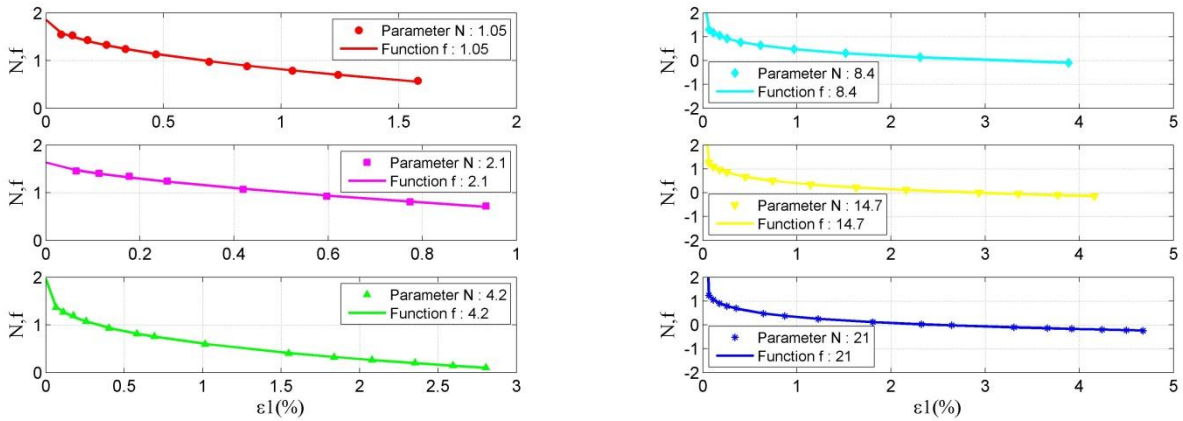

Fig. 5. Plotting the changes of parameter *N* against axial strain □*1* and fitting the function *f* on it in the triaxial compression test on different concrete samples of class C28.6

Table 1. The values of the coefficients of the function *f* for different concrete samples of class C28.6

σ_3 (MPa)	*A*	*B*	*C*
1.05	-1.039	0.4883	1.856
2.1	-0.969	0.6490	1.635
4.2	-1.359	0.3075	1.965
8.4	-2.553	0.1451	3.016
14.7	-4.103	0.0856	4.496
21	-7.929	-0.0443	8.255

The *M* parameter is determined from the experimental results according to Equation (17), and its changes against the ε_1 axial strain are plotted. Then, according to Figure 6, from the fit of the numerical relation 18 on the resulting curves, the numerical coefficients *a*, *b*, *c*, and *d* are calculated and inserted in Table 2 to define the numerical function *g*.

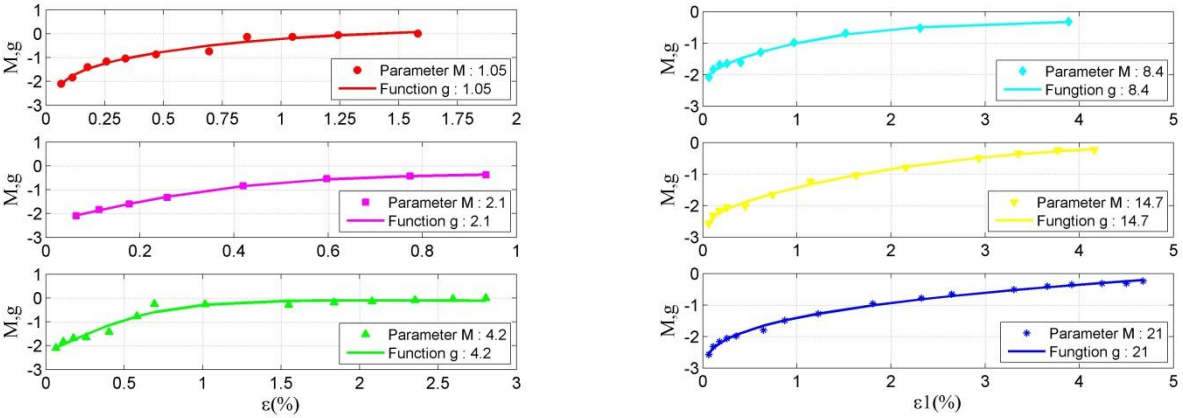

Fig. 6. Plotting the changes of parameter*M* against axial strain□*1* and fitting function*g* on it in thetriaxial compression test on different concrete samples of classC28.6

Table 2. The values of the coefficients of the function *g* for different concrete samples of class C28.6

σ_3 (MPa)	*a*	*b*	*c*	*d*
1.05	-1.050	-0.2663	-1.087	-1.011
2.1	-2.461	0.0100	2.152	2.271
4.2	-2.508	0.0300	-2.478	-1.443
8.4	-1.651	-0.0835	1.161	0.637
14.7	-2.020	-0.0851	1.766	0.348
21	1.985	0.3064	-3.391	185.9

- The modulus of elasticity *E* is determined from Equation (16), and its changes against the axial strain ε_1 are plotted and compared with the experimental results as shown in Figure 7.

-

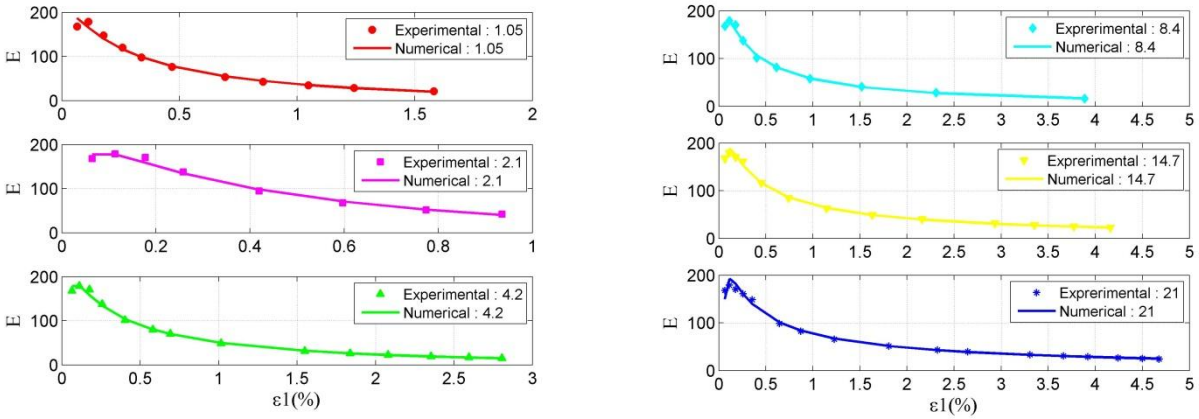

Fig. 7. Diagram of changes $E–\varepsilon_1$ for different concrete samples of class C28.6 and comparison of numerical analysis results with the tri-axial compression test

The Poisson ratio ν is determined from Equation (19), and its variations against the axial strain ε_1 are plotted and compared with the experimental results as shown in Figure 8.

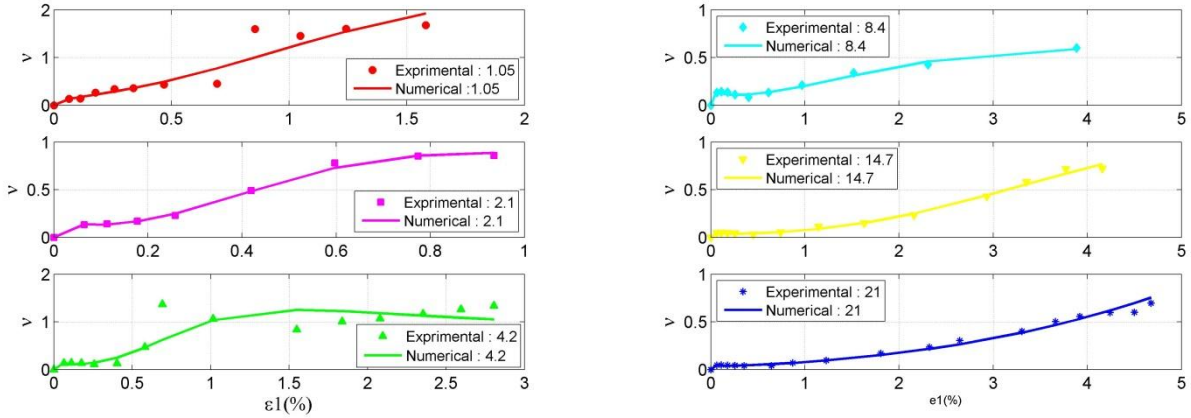

Fig.8. Diagram of $\nu–\varepsilon_1$ changes for different samples of C28.6 class concrete and comparison of numerical analysis results with the tri-axial compression test

Lateral strain ε_3 and volumetric strain ε_v are calculated from equations (5) and (9). The changes in volumetric strain ε_v versus axial strain ε_1 are plotted and, as shown in Figure 9, offer a good agreement with the experimental results.

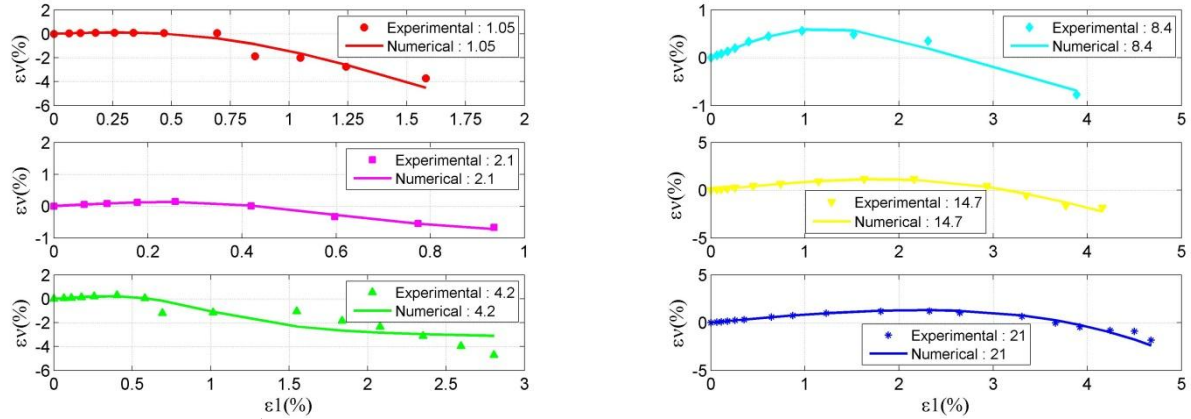

Fig. 9. Diagram of changes $\varepsilon_v–\varepsilon_1$ for different concrete samples of class C28.6 and comparison of numerical analysis results with the tri-axial compression test

The mean and shear stress p and q are determined from equations (10) and (11). The shear stress changes q against the axial strain ε_1 are plotted and, according to Figure 10, show a good agreement with the experimental results.

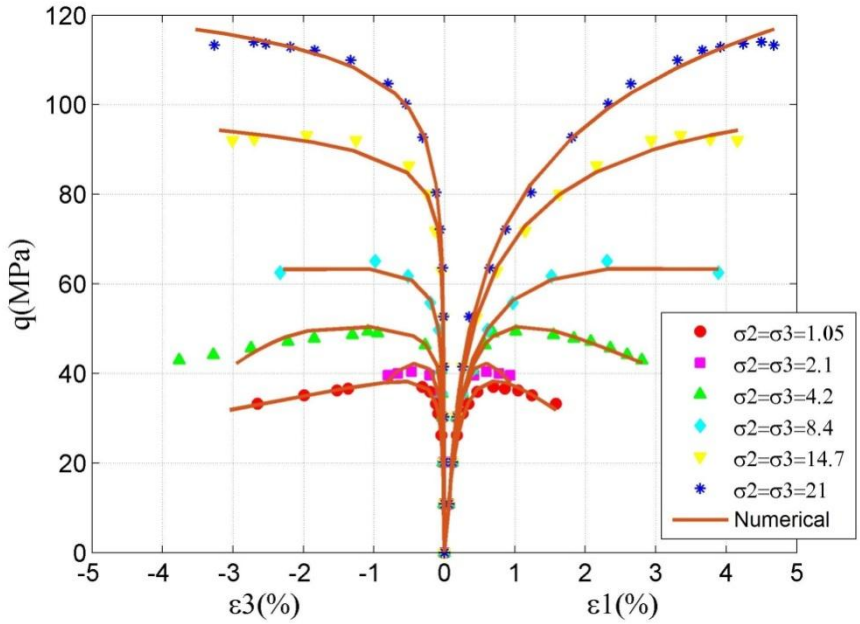

Fig. 10. Diagram of changes $\tilde{q}$ for different concrete samples of class C28.6 and comparison of numerical analysis results with the tri-axial compression test

According to the comparison of recent results, it can be considered appropriate and acceptable to convert the experimental behavior of C28.6 class concrete samples into numerical behavior.

In another study, the results of the triaxial compression test of C60.6 class concrete samples at different confining pressures can be used [51].For this purpose, the numerical analysis parameters for these samples are determined similar to the previous case, and the obtained results are compared with the experimental results. The coefficients obtained in Tables 3 and 4 and the comparative plotting results are presented in Figures 11 to 16.

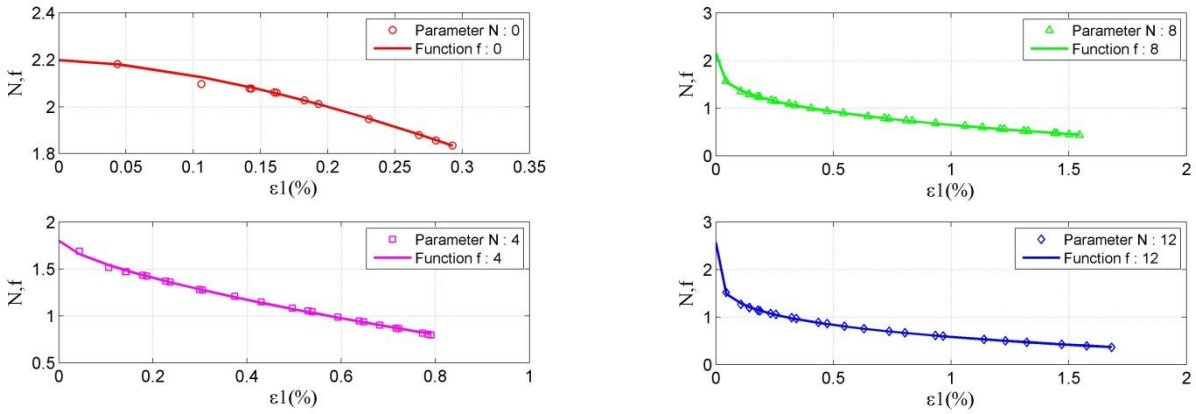

Fig. 11. Plotting the changes of parameter N against axial strain ε_1 and fitting the function f on it in the triaxial compression test on different concrete samples of class C60.6

Table 3. The values of the coefficients of the function f for different concrete samples of class C60.6

σ_3 (MPa)	A	B	C
0	-2.573	1.5900	2.199
4	-1.161	0.6701	1.799
8	-1.504	0.2923	2.151
12	-1.990	0.1952	-29.03

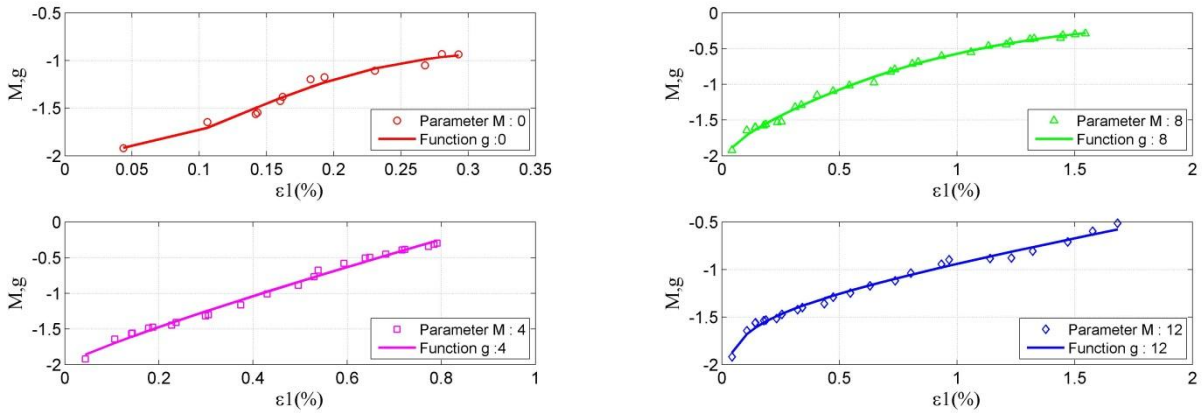

Fig. 12. Plotting the changes of parameter$M$ against axial strainε_1 and fitting function$g$ on it in thetriaxial compression test on different concrete samples of classC60.6

Table 4. The values of the coefficients of the function g for different concrete samples of class C60.6

σ_3 (MPa)	a	b	c	d
0	-8.002	0.3346	5.415	3.7980
4	2.130	0.8701	2.000	-239.00
8	-1.655	-0.0517	1.507	0.9085
12	-1.368	-0.1037	-29.03	-0.0147

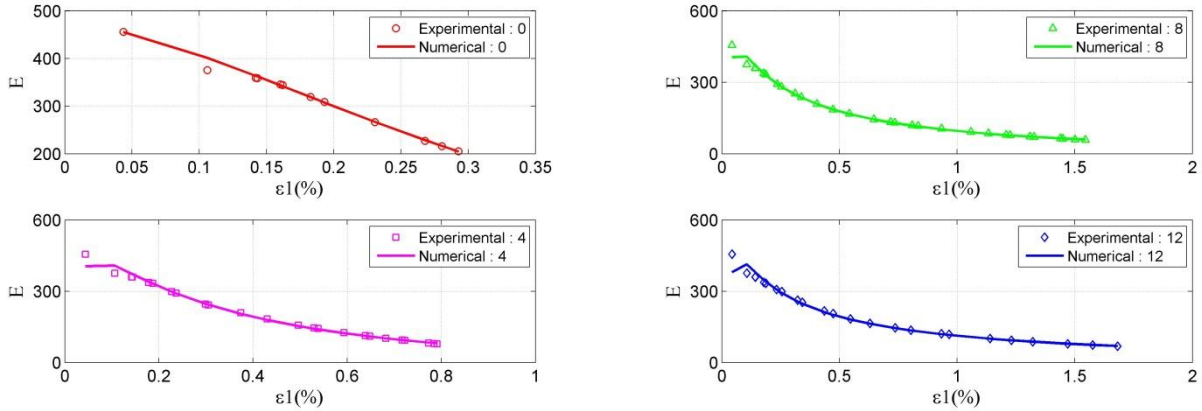

Fig. 13. Diagram of changes $E-\varepsilon_1$ for different concrete samples of class C60.6 and comparison of numerical analysis results with the tri-axial compression test

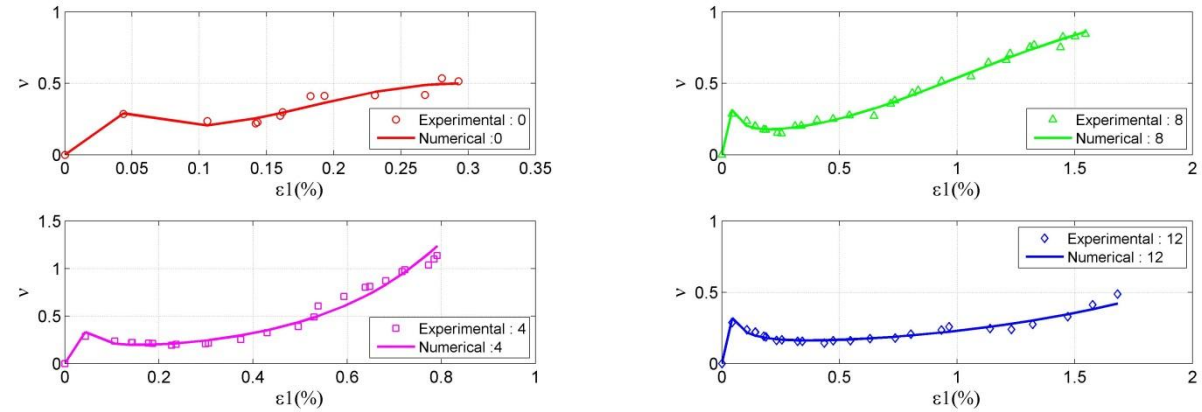

Fig. 14. Diagram of $\nu-\varepsilon_1$ changes for different samples of C60.6 class concrete and comparison of numerical analysis results with the tri-axial compression test

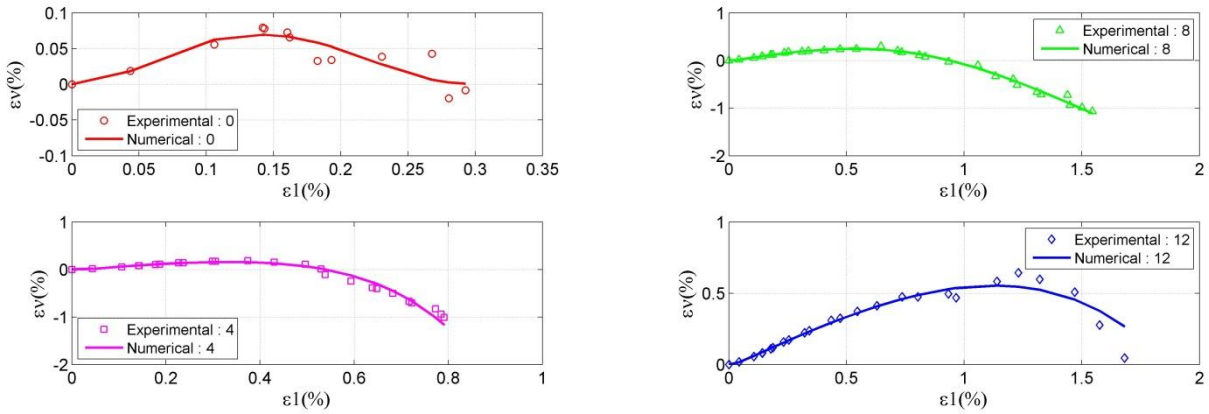

Fig. 15. Diagram of changes ε_v-ε_1 for different concrete samples of class C60.6 and comparison of numerical analysis results with the tri-axial compression test

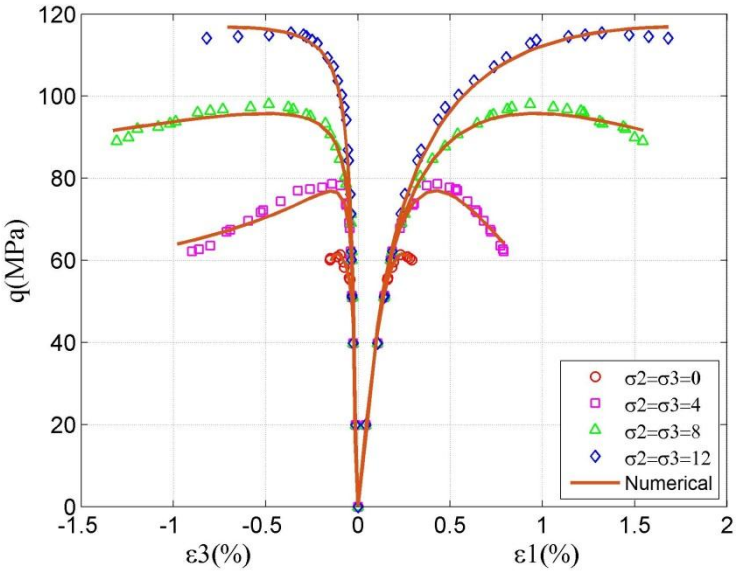

Fig. 16. Diagram of changes q–ε_1 for different concrete samples of class C60.6 and comparison of numerical analysis results with the tri-axial compression test

According to the comparison of recent results, the conversion of the experimental behavior of C60.6 class concrete samples into numerical behavior can be considered appropriate and acceptable.

3.2. Calibration and comparison of numerical analysis results with the uni-axial compression test

In this study, the results of the uni-axial compression test on different classes of concrete can be used [52].For this purpose, the numerical analysis parameters for these samples are determined more easily than before and in conditions $\sigma_3=0$, and the results are compared with experiments. According to the available experimental information, the coefficients obtained in Table 5 and the calibration and graphic comparison results are presented in Figures 17 to 19.

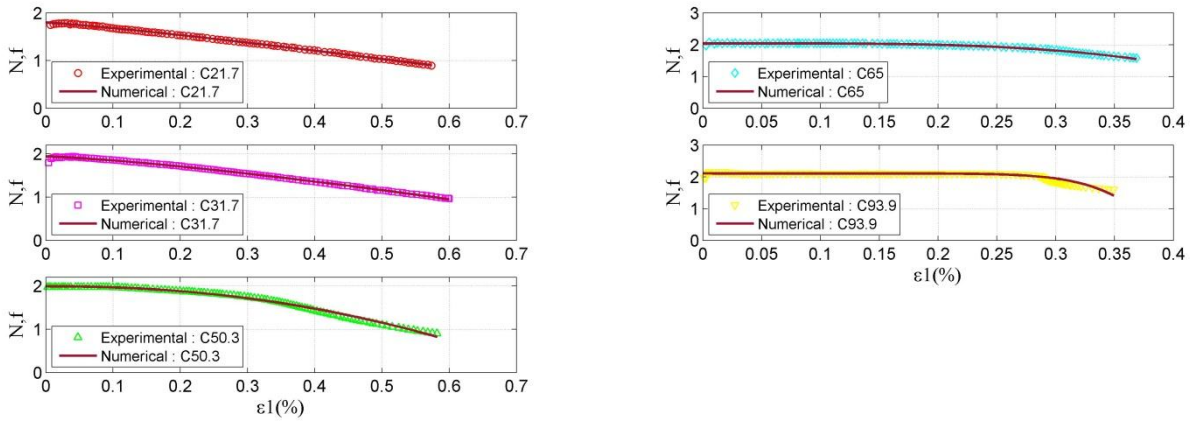

Fig. 17. Plotting the changes of parameter N against axial strain ε_1 and fitting the function f on it in the uni-axial compression test on different classes of concrete

Table 5. The values of the coefficients of the function f for different classes of concrete in the uni-axial compression test

σ_3 (MPa)	A	B	C
211.7	-1.711	1.160	1.799
31.7	-1.945	1.320	1.937
50.3	-3.788	2.172	1.991
65	-22.48	3.822	2.042
93.9	-19830	9.744	2.107

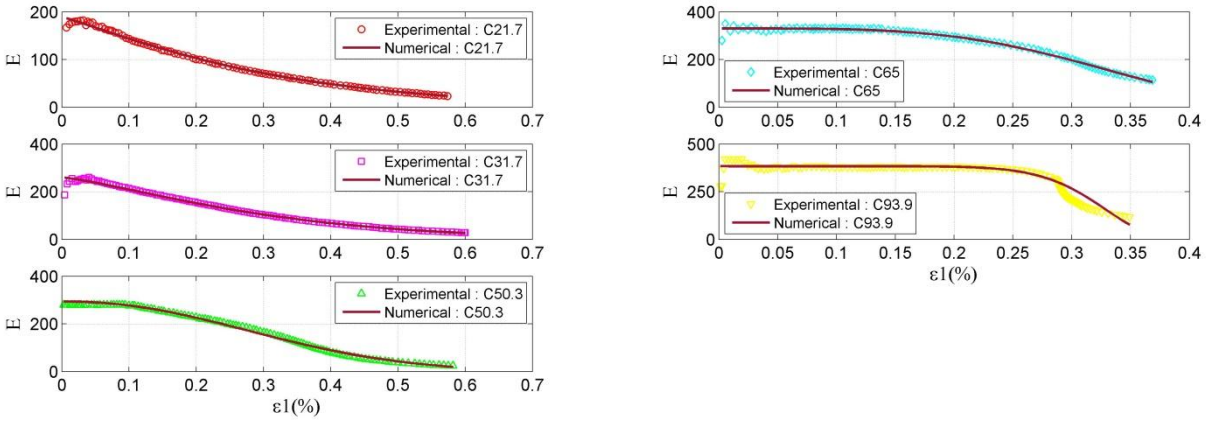

Fig. 18. Diagram of changes E–ε_1 for different classes of concrete and comparison of numerical analysis results with the uni-axial compression test

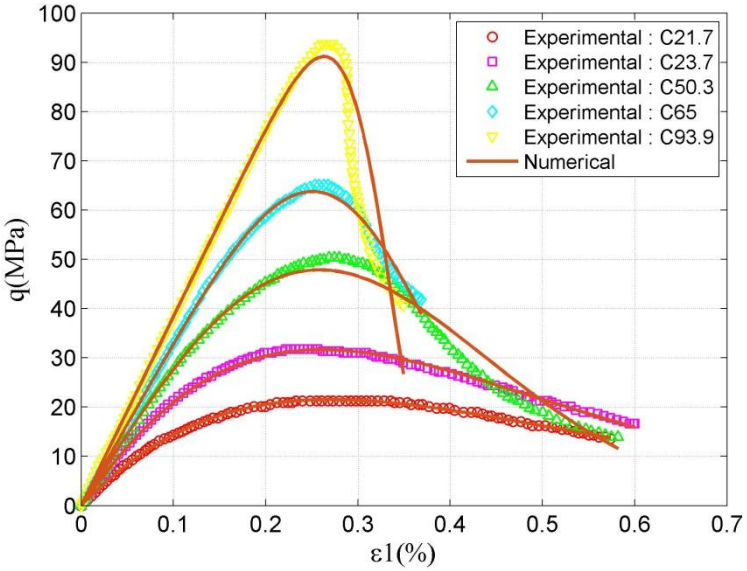

Fig. 19. Diagram of changes $q-\varepsilon_1$ for different classes of concrete and comparison of numerical analysis results with the uni-axial compression test

The conversion of different concrete classes' uni-axial compression experimental behavior into appropriate and acceptable numerical behavior is evaluated.

3.3. Calibration and comparison of numerical analysis results with uni-axial tensile test

In this study, the results of the uni-axial tensile test on different classes of concrete can be used [53].Numerical analysis parameters for these samples are determined similar to the previous case, and the obtained results are compared with the experimental results. According to the available experimental information, the coefficients obtained in Table 6 and the calibration and graphic comparison results are presented in Figures 20 to 22.

Table 6. The values of the coefficients of the function *f* for different classes of concrete in the uni-axial tensile test

σ_3 (MPa)	A	B	C
20	-62.77	0.01	61.96
30	-62.75	0.01	62.03
40	-62.73	0.01	62.09
45	-62.73	0.01	62.11
50	-62.72	0.01	62.12
55	-62.72	0.01	62.15

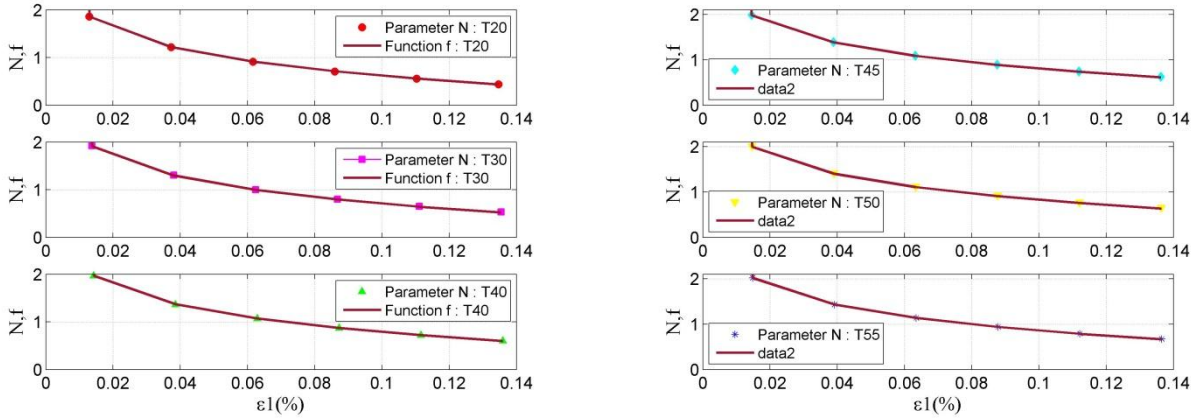

Fig. 20. Plotting the changes of parameter *N* against axial strain ε_1 and fitting the function *f* on it in the uniaxial tensile test on different classes of concrete

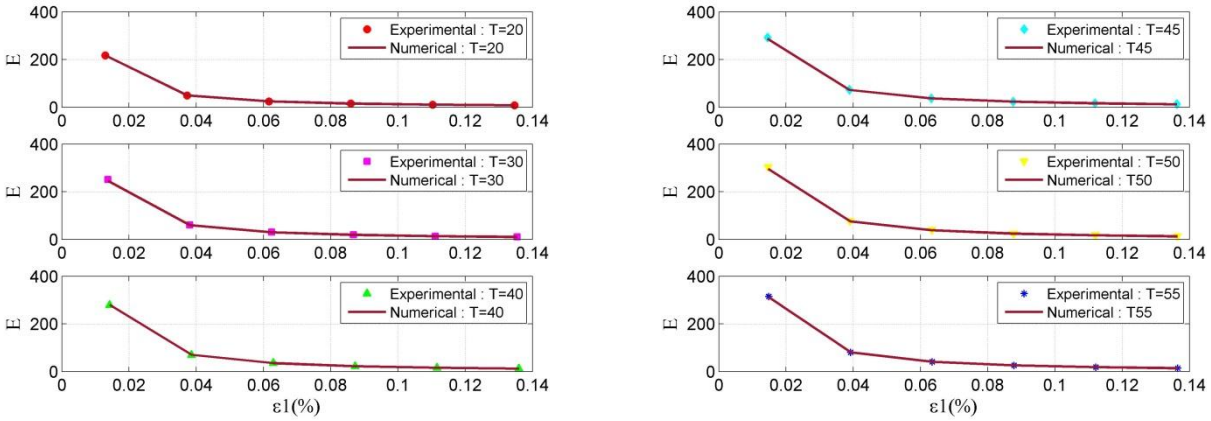

Fig. 21. Diagram of changes $E-\varepsilon_1$ for different classes of concrete and comparison of numerical analysis results with the uni-axial tensile test

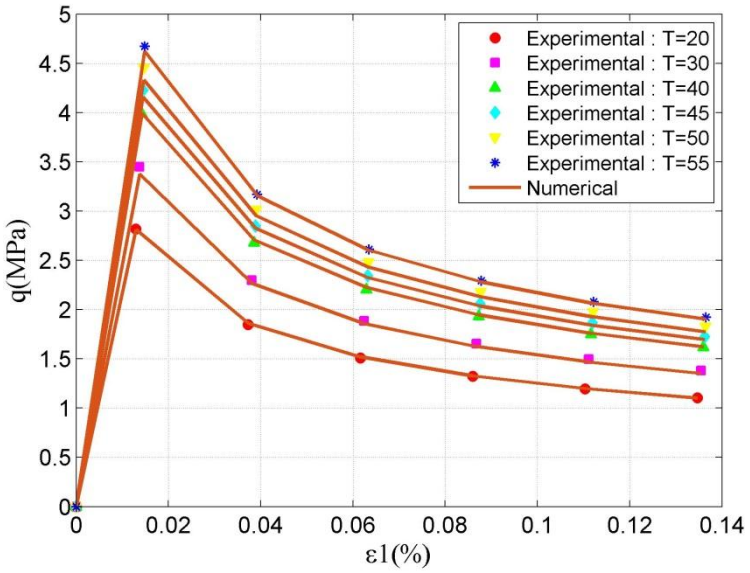

Fig. 22. Diagram of changes $\tilde{q}$, for different classes of concrete and comparison of numerical analysis results with the uni-axial tensile test

The conversion of different concrete classes' uni-axial tensile test behavior to numerical behavior is also considered appropriate.

4. Conclusion

This paper investigated the experimental behavior of different concrete classes in monotonic loading, and hypo-elastic was assumed. Based on the observation of damages in the modulus of elasticity and changes in the Poisson ratio during loading, a numerical and straightforward analytical method was presented to define the linear-nonlinear behavior of concrete. The calibration of this method was evaluated using the related experimental results on different concrete classes. The results of studies, calculations, and comparisons in this research show that designing and achieving this numerical method is valuable. Because it has neither the complexities of micro behavioral models nor the problems of macro behavioral models, it is presented as a simple numerical behavioral analysis. In a general summary, the salient features of this method can be expressed as follows:

1. This numerical method saves time and money with convenient and straightforward computational logic.
2. The function *f* has three coefficients to calculate the damages in the modulus of elasticity, and its calibration is simple with the changes of the experimental parameter *N*.
3. The mathematical relation *g* has four coefficients to calculate the changes in the Poisson ratio, and its calibration with the changes of the experimental parameter *M* requires accuracy.
4. The proposed numerical analysis can present the softening behavior of concrete types. This is not seen in many models or at a high computational cost.
5. Simple numerical analysis process this method is admirable compared to dough models.
6. The proposed numerical method can define the non-isotropic behavior of concrete in pressure, tension and shear and provide more value in multi-laminate models.

It is noteworthy that this numerical method is being completed for other loading modes and placed in multi-laminate models.

References

[1] Aloisio, Angelo, et al. "Indirect assessment of concrete resistance from FE model updating and Young's modulus estimation of a multi-span PSC viaduct: Experimental tests and validation." *Structures*. Vol. 37. Elsevier, 2022.

[2] Xu, J. J., et al. "A Bayesian model updating approach applied to mechanical properties of recycled aggregate concrete under uniaxial or triaxial compression." *Construction and Building Materials* 301 (2021): 124274.

[3] Vu, Chi-Cong, et al. "Revisiting statistical size effects on compressive failure of heterogeneous materials, with a special focus on concrete." *Journal of the Mechanics and Physics of Solids* 121 (2018): 47-70.

[4] Pijaudier-Cabot, Gilles, and Zdeněk P. Bažant. "Nonlocal damage theory." *Journal of engineering mechanics* 113.10 (1987): 1512-1533.

[5] Pastor, M., O. C. Zienkiewicz, and AHC0702 Chan. "Generalized plasticity and the modelling of soil behaviour." *International Journal for numerical and analytical methods in geomechanics* 14.3 (1990): 151-190.
[6] Jirasek, Milan. "Nonlocal models for damage and fracture: comparison of approaches." *International Journal of Solids and Structures* 35.31-32 (1998): 4133-4145.
[7] Lee, K. M., and J. H. Park. "A numerical model for elastic modulus of concrete considering interfacial transition zone." *Cement and Concrete Research* 38.3 (2008): 396-402.
[8] Jayawardhana, Madhuka, X. Q. Zhu, and RanjithLiyanapathirana. "An experimental study on damage detection of concrete structures using decentralized algorithms." *Advances in Structural Engineering* 16.1 (2013): 33-50.
[9] Jefferson, A. D., et al. "A plastic-damage-contact constitutive model for concrete with smoothed evolution functions." *Computers & Structures* 169 (2016): 40-56.
[10] Wang, Guosheng, et al. "A true 3D frictional hardening elastoplastic constitutive model of concrete based on a unified hardening/softening function." *Journal of the Mechanics and Physics of Solids* 119 (2018): 250-273.
[11] Bažant, Zdeněk P., and Byung H. Oh. "Microplane model for progressive fracture of concrete and rock." *Journal of Engineering Mechanics* 111.4 (1985): 559-582.
[12] Bažant, Zdeněk P., and Pere C. Prat. "Microplane model for brittle-plastic material: I. Theory." *Journal of Engineering Mechanics* 114.10 (1988): 1672-1688.
[13] SADREJAD, SA, and G. N. Pande. "A multilaminate model for sands." *International symposium on numerical models in geomechanics. 3 (NUMOG III)*. 1989.
[14] Baz a ˇ nt, Zdeněk P., and JoškoOžbolt. "Nonlocal microplane model for fracture, damage, and size effect in structures." *Journal of Engineering Mechanics* 116.11 (1990): 2485-2505.
[15] Sadrnejad, S. A. "Multilaminateelastoplastic model for granular media." *International Journal of Engineering* 5.1 (1992): 11-24.
[16] Bazant, Zdenek P., and JoskoOzbolt. "Compression failure of quasibrittle material: Nonlocal microplane model." *Journal of engineering mechanics* 118.3 (1992): 540-556.
[17] Ožbolt, Joško, and Zdeněk P. Bažant. "Microplane model for cyclic triaxial behavior of concrete." *Journal of engineering mechanics* 118.7 (1992): 1365-1386.
[18] Carol, Ignacio, Pere C. Prat, and Zdeněk P. Bažant. "New explicit microplane model for concrete: theoretical aspects and numerical implementation." *International Journal of Solids and Structures* 29.9 (1992): 1173-1191.
[19] Bažant, Zdeněk P., Yuyin Xiang, and Pere C. Prat. "Microplane model for concrete. I: Stress-strain boundaries and finite strain." *Journal of Engineering Mechanics* 122.3 (1996): 245-254.
[20] Bažant, Zdeněk P., et al. "Microplane model for concrete: II: data delocalization and verification." *Journal of Engineering Mechanics* 122.3 (1996): 255-262.
[21] Bažant, Zdeněk P., et al. "Microplane model M4 for concrete. I: Formulation with work-conjugate deviatoric stress." *Journal of Engineering Mechanics* 126.9 (2000): 944-953.
[22] Sadrnejad, SeyedAmirodin, and Hamid Karimpour. "Drained and undrained sand behaviour by multilaminate bounding surface model." *International Journal of Civil Engineering* 9.2 (2011): 111-125.
[23] Daouadji, Ali, et al. "Experimental and numerical investigation of diffuse instability in granular materials using a microstructural model under various loading paths." *Géotechnique* 63.5 (2013): 368-381.
[24] Fang, H. L., H. Zheng, and Jun Zheng. "Micromechanics-based multimechanism bounding surface model for sands." *International Journal of Plasticity* 90 (2017): 242-266.
[25] Keerthana, K., and JM Chandra Kishen. "Micromechanics of fracture and failure in concrete under monotonic and fatigue loadings." *Mechanics of Materials* 148 (2020): 103490.
[26] Lu, Dechun, et al. "A cohesion-friction combined hardening plastic model of concrete with the nonorthogonal flow rule: Theory and numerical implementation." *Construction and Building Materials* 325 (2022): 126586.
[27] Zheng, B. T., and J. G. Teng. "A plasticity constitutive model for concrete under multiaxial compression." *Engineering Structures* 251 (2022): 113435.
[28] Bakhti, R., et al. "New approach for computing damage parameters evolution in plastic damage model for concrete." *Case Studies in Construction Materials* 16 (2022): e00834.
[29] Jin, Liu, et al. "Numerical and theoretical investigation on the size effect of concrete compressive strength considering the maximum aggregate size." *International Journal of Mechanical Sciences* 192 (2021): 106130.
[30] Zhou, Xin, et al. "A 3D non-orthogonal plastic damage model for concrete." *Computer Methods in Applied Mechanics and Engineering* 360 (2020): 112716.
[31] Poliotti, Mauro, and Jesús-Miguel Bairán. "A new concrete plastic-damage model with an evolutivedilatancy parameter." *Engineering structures* 189 (2019): 541-549.
[32] Mohammadi, Mohsen, and Yu-Fei Wu. "Modified plastic-damage model for passively confined concrete based on triaxial tests." *Composites Part B: Engineering* 159 (2019): 211-223.
[33] Sarikaya, A., and R. E. Erkmen. "A plastic-damage model for concrete under compression." *International Journal of Mechanical Sciences* 150 (2019): 584-593.

[34] Demin, Wei, and He Fukang. "Investigation for plastic damage constitutive models of the concrete material." *Procedia engineering* 210 (2017): 71-78.
[35] Wu, Zhangyu, et al. "Mesoscopicmodelling of concrete material under static and dynamic loadings: A review." *Construction and Building Materials* 278 (2021): 122419.
[36] Xia, Yang, et al. "Mesoscopic study of concrete with random aggregate model using phase field method." *Construction and Building Materials* 310 (2021): 125199.
[37] Jin, Liu, et al. "Mesoscopic simulations on the strength and size effect of concrete under biaxial loading." *Engineering Fracture Mechanics* 253 (2021): 107870.
[38] Li, Dong, et al. "Theoretical characterization of mesoscopic dynamic fracture behaviors of concrete based on an extended self-consistent finite stress model (XSFSM)." *Theoretical and Applied Fracture Mechanics* 108 (2020): 102677.
[39] Peyman, Farzad, and Seyed A. Sadrnejad. "Analysis of concrete crack growth based on micro-plane model." *Structural Concrete* 19.3 (2018): 930-945.
[40] Kwan, A. K. H., P. L. Ng, and Z. M. Wang. "Mesoscopic analysis of crack propagation in concrete by nonlinear finite element method with crack queuing algorithm." *Procedia Engineering* 172 (2017): 620-627.
[41] Sadrnejad, S. A., and ShShakeri. "Multi-laminate non-coaxial modelling of anisotropic sand behavior through damage formulation." *Computers and Geotechnics* 88 (2017): 18-31.
[42] Sadrnejad, S. A., and ShShakeri. "Fabric assessment of damaged anisotropic geo-materials using the multi-laminate model." *International Journal of Rock Mechanics and Mining Sciences* 91 (2017): 90-103.
[43] Negi, Alok, and Sachin Kumar. "A continuous–discontinuous localizing gradient damage framework for failure analysis of quasi-brittle materials." *Computer Methods in Applied Mechanics and Engineering* 390 (2022): 114434.
[44] Peng, Rong-xin, Wen-liangQiu, and Meng Jiang. "Application of a micro-model for concrete to the simulation of crack propagation." *Theoretical and Applied Fracture Mechanics* 116 (2021): 103081.
[45] Stamati, O., et al. "Fracturing process of micro-concrete under uniaxial and triaxial compression: Insights from in-situ X-ray mechanical tests." *Cement and Concrete Research* 149 (2021): 106578.
[46] Wu, Baijian, Zhaoxia Li, and Keke Tang. "Numerical modeling on micro-to-macro evolution of crack network for concrete materials." *Theoretical and Applied Fracture Mechanics* 107 (2020): 102525.
[47] Nguyen, Tuan, et al. "Uncertainty quantification of the mechanical properties of lightweight concrete using micromechanical modelling." *International Journal of Mechanical Sciences* 173 (2020): 105468.
[48] Alam, Syed Yasir, and Ahmed Loukili. "Effect of micro-macro crack interaction on softening behaviour of concrete fracture." *International Journal of Solids and Structures* 182 (2020): 34-45.
[49] Evangelista Jr, Francisco, and José FabianoAraújo Moreira. "A novel continuum damage model to simulate quasi-brittle failure in mode I and mixed-mode conditions using a continuous or a continuous-discontinuous strategy." *Theoretical and Applied Fracture Mechanics* 109 (2020): 102745.
[50] Imran, Iswandi. "Applications of non-associated plasticity in modelling the mechanical response of concrete." (1996): 3905-3905.
[51] Candappa, D. C., J. G. Sanjayan, and SujeevaSetunge. "Complete triaxial stress-strain curves of high-strength concrete." *Journal of materials in civil engineering* 13.3 (2001): 209-215.
[52] Dahl, Kaare KB. *A constitutive model for normal and high strength concrete*. Afdelingen for BaerendeKonstruktioner, DankmarksTekniskeHøjskole, 1992.
[53] Červenka, Jan, and Vassilis K. Papanikolaou. "Three dimensional combined fracture–plastic material model for concrete." *International journal of plasticity* 24.12 (2008): 2192-2220.